Two Models for Hard Braking Vehicles and Collision Avoiding Trajectories

Fynn Terhar

BMW Group / FernUniversität in Hagen
Department for Fleet Intelligence
Munich, Germany
Email: fynn.terhar@bmw.de

Christian Icking

FernUniversität in Hagen
Department for Cooperative Systems
Hagen, Germany
Email: christian.icking@fernuni-hagen.de

***Abstract*—In this paper, we describe two models that describe vehicle dynamics in full braking situations with collision avoiding motions. By combining the equations of the classic Ackermann-Model with conditions that ensure a stable vehicle movement during simultaneous heavy braking and turning motions, we derive two models that describe the set of controllable trajectories by compound equations in the x, y plane. We describe a simplified model first and compare its performance to the well known Constant-Turn-Rate-And-Acceleration-Model, which is computationally more expensive and less precise. We discuss the simplified model regarding uncertainties and their effect on reachability estimation of vehicles in admissible scenarios, to show the feasibility of our solution. By considering uncertainties of the parameters used in the Basic Model, we show a way to estimate the reachable area of a hard braking vehicle in different starting constellations. We extend this Basic Model to handle much more dynamic situations and starting conditions. In the new Extended Model, the initial yaw rate is an input, as well as the maximum steering angle change rate. The vehicle length and steering direction are also considered. By these additions, we are able to describe trajectories in much more realistic detail than with the Basic Model. We derive and present all necessary equations required for computing these trajectories. Furthermore, we analyze and demonstrate all possible types of trajectories that directly follow from our definitions.**

Keywords–Reachability; Trajectory; Dynamic Vehicle Model; Safety; Collision Avoidance; Braking; Trajectory Types.

I. Introduction

Many functions in Highly Automated Driving (HAD) and Advanced Driving Assistance Systems (ADAS) are discussed regarding their safety towards events caused by other traffic participants, whose behavior is not well predictable. In case of an unforeseen event, vehicles need to avoid a collision by a suitable trajectory. In literature, these trajectories are often referred to as Fail-Safe-Trajectories. These trajectories can either be evasive and try to find a solution around an obstacle or bring the vehicle to an emergency stop. The vehicle is then forced to find a trajectory till full stop within an area in front of the vehicle, which is defined by its physical properties and speed vector.

A. Motivation

In this paper, we call this area the *Braking Area*, which is important to know in many different applications and situations, such as in Figure 1, in which two vehicles are unexpectedly confronted with each other. Also, when defining the set up of on-board sensors, it can be useful to have a good knowledge of the braking area. Another example is the search for fail-safe trajectories, such as shown in Figure 2, where the knowledge of the reachable set of vehicle states can significantly accelerate the computation, as it reduces the search space and can therefore save valuable time in emergency situations.

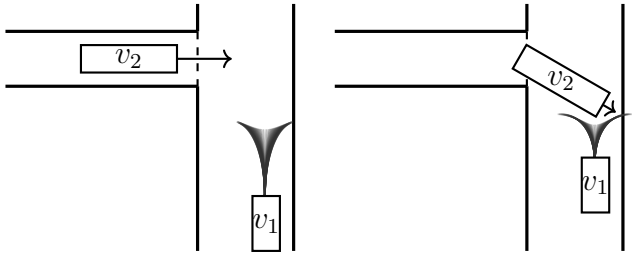

Figure 1. Left, two vehicles v_1, v_2 approach a crossing. Right, at sudden confrontation, v_1 can benefit from its reachable area for emergency braking.

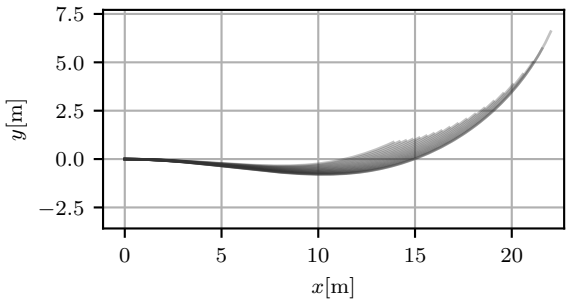

Figure 2. A set of 20 braking trajectories computed by the Extended Model introduced in this paper. Advanced dynamics at the start state are incorporated.

B. Literature overview

This paper is based on our previous work introduced in [1], where we introduce a new model to compute trajectories of hard braking and collision avoiding vehicles. This task is related to finding fail-safe trajectories. Methods for avoiding obstacles are numerous, see for example Werling et al. [2], where the authors address dynamic street scenarios by an optimal control approach. The method generates trajectories that are optimal in terms of jerk minimization and following a previously computed trajectory. Another approach is explained by Ziegler et al. [3]. They use a cost function to plan obstacle avoiding paths in unstructured environments, but not on the

description of fail-safe trajectories. Several approaches towards finding fail safe trajectories for road vehicles exist. Pek and Althoff [4] describe a method to generate fail-safe trajectories for dynamic traffic scenarios in a computationally efficient manner. Their solution approximates the set of reachable states of the ego vehicle and other traffic participants and can therefore guarantee collision free trajectories. A motion planner for fail-safe trajectories is shown by Magdici and Althoff [5]. A related application is presented in [6], where a safety framework is demonstrated that can test a planned trajectory for possible future collisions. A complete motion planning system is described by Heinrich [7]. The presented sampling based approach consists of three cyclic, elementary steps. State Space Exploration uses vehicle surround view sensors. Based on the explored state space, trajectory samples are generated during Trajectory Generation phase. The last step consists in Optimization, which means finding an optimal trajectory from the previously generated trajectories.

Mitchell et al. [8] discuss different approaches of reachability analysis of dynamic systems for the safety assessment of trajectories. Asarin et al. [9] present an approach for reachability approximation of partially linearized systems in general. An often applied technique to approximate the state space efficiently is by zonotopes, see, e.g., the paper of Girad [10]. Koschi et al. [11] introduce an open source software solution which predicts road occupancy by traffic participants within a given time horizon. By overestimating the occupancy by the union of several object models, the authors ensure to find all possible traffic configurations. Potential braking and turning is overestimated by a circle of lateral and longitudinal maximum and minimum accelerations. The physical interaction between velocity and admissible lateral accelerations are therefore overestimated. Althoff [12] describes many underlying concepts of reachability analysis for road vehicles. In contrast to formal verification, ByeoungDo et al. [13] propose a Recurrent Neural Net for predicting traffic participants. Explicit braking and turning motions and their interrelation are not in the focus. Both of our models provide a more detailed and accurate description of this interaction in order to reduce the overestimation towards a more realistic model.

The interrelation of braking and turning is, e.g., discussed by Giovannini et al. [14] where the authors describe the last point in time when a collision can be avoided by swerving. The authors explicitly focus their work on two-wheeled vehicles. Ackermann et al.[15] present control strategies for braking and swerving motions. Choi et al. [16] propose an additional strategy based on model predictive control.

C. Contribution

In this paper, we present two different models for calculating feasible trajectories for braking while turning. In the first part, we describe a Basic Model that can quickly calculate motion primitives for estimating the reachable area of a vehicle while simultaneously braking and turning, further on called *Braking Area*. This *Basic Model* is simplified in two essential points. Firstly, the yaw rate at time $t = 0$, which is the change in direction a vehicle is pointing, was implicitly assumed to be zero. Secondly, the rate at which the yaw rate $\dot{\psi}$ can change, was assumed to be ∞. In order to estimate the Braking Area, these assumptions are valid as they include all trajectories with more realistic properties, and hence lead to an acceptable overestimation of the breaking area. However, when calculating feasible braking trajectories in scenarios that deviate much from the aforementioned assumptions, a more realistic model is to be preferred. Therefore, we extend the Basic Model towards an *Extended Model* by including the yaw rate at time $t = 0$ as $\dot{\psi}_0$, as well as a new model parameter $\dot{\hat{\delta}}$, which limits the change rate of $\dot{\psi}$ by changing the steering angle δ. See Figure 2 for an example in which a set of Extended Model trajectories are shown. Furthermore, we extend the Basic Model by the turning direction s, which determines the sign of a trajectory's curvature. With these extensions, we drastically raise the applicability towards being able to:

1) Calculate realistic trajectories, also for dynamic situations at $t = 0$.
2) Call the model recursively, as all produced outputs my be fed back as inputs.
3) Use the model to calculate motion primitives for any start state of moving vehicles which is in a stable state, e.g., is not sliding over the road uncontrollably.
4) Search for feasible and yet complex emergency trajectories by concatenating motion primitives.

With these two models, we contribute equations that can be used to calculate trajectories for automated vehicles or to estimate the reachable area in emergency braking situations. With respect to the work of Heinrich [7], our equations contribute trajectories for the Trajectory Generation step of vehicle motion planning for automated driving.

In Section II, we describe underlying assumptions that hold for both models and outline the major differences. Used symbols and notations are also described. In Section III we derive the Basic Model, which directly calculates vehicle trajectories towards a full stop while simultaneously braking and steering under simplified assumptions. Section III-A introduces all equations of the Basic Model. Braking and steering always needs to be performed in a balanced way, as both influence the controllability of the vehicle on the road. We therefore introduce a parameter that describes the ratio of this compromise. Furthermore, the friction between different road surfaces and tires is considered. A comparison of the introduced Basic Model and the CTRA-Model is given in Section III-B. The influence that uncertain model inputs and parameters have are discussed in Section III-C. The Extended Model is introduced in Section IV. The model equations of the Extended Model are derived in Section IV-A, which takes the change rate of steering angle into account, as well as the turning direction of the vehicle and the initial yaw rate and the maximum change in steering angle combined with the vehicle length. Subsequently, Section IV-B analyzes and determines all possible types of trajectories that directly follow from our equations. Each trajectory is characterized formally and demonstrated by example trajectories. At last, Section V discusses the applicability and further research regarding the models defined in this paper.

II. Definitions for the Two Models and Their Differences

In this section, we describe all symbols of the two models and common assumptions.

Physical model values are denoted as regular latin letters, while angles are denoted as greek letters. Symbols used in this paper are summarized in the following Table I.

TABLE I. SYMBOLS AND NOTATION USED IN THIS PAPER.

Symbol	*Description*	*Unit*
X_i	Model state at time i	–
p	Position $\in \mathbb{R}^2$	m
X_{stop}	Stop state, $v = 0$	–
ψ	Yaw Angle	rad
$\dot{\psi}$	Yaw Rate	rad/s
s	Direction of steering as sign ± 1	–
$\dot{\hat{\delta}}$	Maximal steering angle change	rad/s
δ	Steering angle	rad
b	Braking Factor	–
$\hat{a}$	Maximum admissible acceleration	m/s^2
r_{turn}	Minimum turning radius	m
L	Length of a vehicle	m
$\mathcal{I}_\bullet$	Interval of admissible values for $\bullet$	–
$\bullet_{\min}, \bullet_{\max}$	Extreme values of $\mathcal{I}_\bullet$	–
$f_{\text{T}}(t), f_{\text{F}}(t), f_{\text{R}}(t)$	Part of $f(t)$ limited by **T**urning, **F**riction, **R**adius	–
$\widetilde{F}(t)$	Integral without constant: $\widetilde{F}(t) = \int f(t)dt - C_{\text{F}}$	–
$\overline{f}(t)$	Linearized version of $f(t)$	–
$f_x = f(t_x)$	Abbreviating function values of f at times t_x	–
$\mathcal{S}(t), \mathcal{C}(t)$	Sine and Cosine Fresnel Function[17]	–

Both models assume an ordered priority, on which the trajectory calculations are based upon:

1) The vehicle needs to be brought into a state with velocity $v = 0$ quickly.
2) Steering dynamics may be used to avoid obstacles or to reduce unavoidable impact.

In Figure 3, the main difference of the two models can be seen. The Extended Model takes the initial yaw rate $\dot{\psi}_0$ into consideration, which leads to three additional model parameters compared to the Basic Model, namely the maximum steering angle change rate $\dot{\hat{\delta}}$, the direction of steering as sign s and the vehicle length L.

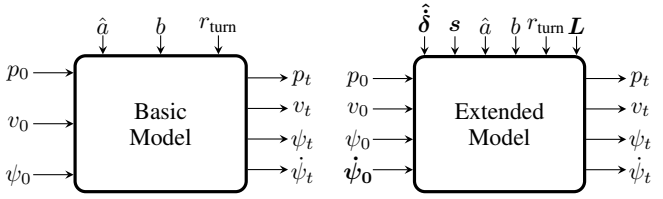

(a) Basic Model without initial yaw rate and steering dynamics.

(b) Extension with one additional input and three additional parameters.

Figure 3. A comparison of both model's parameters (top) and state inputs (left). Note that model outputs (right) are the same in both models.

III. BASIC MODEL

This section describes the Basic Model, in which no initial yaw rate $\dot{\psi}_0$ is incorporated, however a maximal steering angle change rate $\dot{\hat{\delta}}$ of ∞ is assumed, which is sufficient for reachability estimation. A black box view of the model is shown in Figure 3a.

A. Equations of the Basic Model

The Basic Model is based on the so called *Friction Circle*, e.g., described by Pacejka [18]. As the modeled vehicle is braking in order to come to a full stop quickly, it will always be located near the boundary of this circle, either due to braking only, or by braking and turning in combination, as shown in Figure 4. The circle defines controllability when Equation (1) holds, where $\vec{a}_{\text{lon}}$ is the longitudinal acceleration component and $\vec{a}_{\text{cen}}$ the centripetal component, respectively.

$$\hat{a} \geq \|\vec{a}_{\text{res}}\| = \|\vec{a}_{\text{lon}} + \vec{a}_{\text{cen}}\| \tag{1}$$

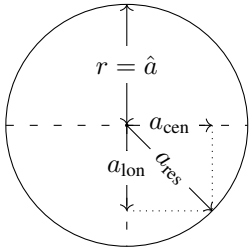

Figure 4. Friction Circle in the a_x, a_y-plane. Radius r is equal to the maximally applicable acceleration $\hat{a}$ between vehicle and road surface.

As the acceleration a_{res} results from a combination of braking and steering, the ratio $a_{\text{lon}}/\hat{a}$ causes different trajectories. We define this ratio by the factor b, as declared in Equation (2), further on called *Braking Factor*. We call b Braking Factor, as it describes the percentage of $\hat{a}$ that is applied for braking rather than turning. A b value of -0.5 means that 50% of the applicable acceleration is applied for braking. Note that $\hat{a}$ is positive, but when braking a_{lon} is negative, hence we choose $b \in [-1, 0]$.

$$b := \frac{a_{\text{lon}}}{\hat{a}} \tag{2}$$

The Basic Model provides a formal description of vehicle position $p(t) = [x, y]^T$ which is generally defined by the following integral:

$$p(t) = \begin{bmatrix} x(t) \\ y(t) \end{bmatrix} = \int v(t) \begin{bmatrix} \cos(\psi(t)) \\ \sin(\psi(t)) \end{bmatrix} dt \tag{3}$$

where

$$v(t) = a_{\text{lon}} t + v_0 \tag{4}$$

A definition of $\psi(t)$ can be found by integrating the yaw rate $\dot{\psi}(t)$ over time t. In this Basic Model, the yaw rate is constrained by two different limits. The first limit is the Friction Circle, which does not allow higher yaw rates due to an otherwise resulting instable trajectory. This yaw rate is called $\dot{\psi}_{\text{F}}$. The second limit for the yaw rate is caused by the minimum turning radius r_{turn}. We call it $\dot{\psi}_{\text{R}}$. We thus define the yaw rate stepwise as given in Equation (5).

$$\dot{\psi}(t) = \begin{cases} \dot{\psi}_{\text{F}}(t) = \frac{\hat{a}\sqrt{1-b^2}}{v(t)}, & 0 \leq t \leq t_{\text{FR}} \\ \dot{\psi}_{\text{R}}(t) = \frac{v(t)}{r_{\text{turn}}}, & t_{\text{FR}} < t \leq t_{\text{stop}} \end{cases}, \forall t \geq 0 \tag{5}$$

where t_{FR} is defined as the time of intersection between $\dot{\psi}_{\text{F}}(t)$ and $\dot{\psi}_{\text{R}}(t)$ as can be seen in Equation (6) and t_{stop} is the time when $v = 0$ (see Equation (7)).

$$t_{\text{FR}} = \max\left(a_{\text{lon}}^{-1}\left(\sqrt{r_{\text{turn}}\hat{a}\sqrt{1-b^2}} - v_0\right), 0\right) \tag{6}$$

$$t_{\text{stop}} = -v_0 a_{\text{lon}}^{-1} \tag{7}$$

The yaw angle over time is then simply the time integral over $\dot{\psi}(t)$, as shown in Equation (8).

$$\psi(t) = \int \dot{\psi}(t)dt = \begin{cases} \psi_{\mathrm{F}}(t), & 0 \leq t \leq t_{\mathrm{FR}} \\ \psi_{\mathrm{R}}(t), & t_{\mathrm{FR}} < t \leq t_{\mathrm{stop}} \end{cases}, \forall t \geq 0 \quad (8)$$

where

$$\psi_{\mathrm{F}}(t) = z(\ln(v(t)) - \ln(v_0)) + \psi_0 \quad (9)$$

$$\psi_{\mathrm{R}}(t) = \left(\frac{1}{2}a_{\mathrm{lon}}t^2 + v_0 t\right) r_{\mathrm{turn}}^{-1} + C_{\psi,\mathrm{R}} \quad (10)$$

$$z = b^{-1}\sqrt{1-b^2} \quad (11)$$

$$C_{\psi,\mathrm{R}} = \psi_{\mathrm{F}}(t_{\mathrm{FR}}) - \left(\frac{1}{2}a_{\mathrm{lon}}t^2 - v_0 t\right) r_{\mathrm{turn}}^{-1} \quad (12)$$

Here, $C_{\psi,\mathrm{R}}$ is the constant of integration. With these equations, a solution for the positional integrals $x(t)$ and $y(t)$ can be found as shown in Equations (15) and (20). The x-Position can be calculated by Equations (13) and (14):

$$x_{\mathrm{F}}(t) = \frac{v(t)^2\left(z\sin(\psi(t)) + 2\cos(\psi(t))\right)}{a_{\mathrm{lon}}\left(z^2+4\right)} + C_{\mathrm{x,F}} \quad (13)$$

$$x_{\mathrm{R}}(t) = r_{\mathrm{turn}}\sin(\psi(t)) + C_{\mathrm{x,R}} \quad (14)$$

These equations describe position over time $x(t)$ and $y(t)$. See stepwise Equation (15) for $x(t)$.

$$x(t) = \begin{cases} x_{\mathrm{F}}(t), & 0 \leq t \leq t_{\mathrm{FR}} \\ x_{\mathrm{R}}(t), & t_{\mathrm{FR}} < t \leq t_{\mathrm{stop}} \end{cases} \quad (15)$$

The constant $C_{\mathrm{x,F}}$ is bound by the conditions $x(0) = x_0$, which means the vehicle must be at the starting position at time t_0. The constant for x_{F}, $C_{\mathrm{x,F}}$, is bound to hold the condition $x_{\mathrm{R}}(t_{\mathrm{FR}}) = x_{\mathrm{F}}(t_{\mathrm{FR}})$, which means that $x_{\mathrm{F}}(t)$ must seamlessly – e.g., in value and gradient – be continued by $x_{\mathrm{R}}(t)$ at t_{FR}. The result for both constants is described by Equations (16) and (17).

$$C_{\mathrm{x,F}} = x_0 - \frac{v_0^2\left(z\sin(\psi_0) + 2\cos(\psi_0)\right)}{a_{\mathrm{lon}}(z^2+4)} \quad (16)$$

$$C_{\mathrm{x,R}} = x(t_{\mathrm{FR}}) - r_{\mathrm{turn}}\sin(\psi(t_{\mathrm{FR}})) \quad (17)$$

The general description for $y(t)$ is shown below in Equation (20), while the step wise segments of all y-positions are shown in Equations (18) and (19):

$$y_{\mathrm{F}}(t) = -\frac{v(t)^2\left(z\cos(\psi(t)) - 2\sin(\psi(t))\right)}{a_{\mathrm{lon}}\left(z^2+4\right)} + C_{\mathrm{y,F}} \quad (18)$$

$$y_{\mathrm{R}}(t) = -r_{\mathrm{turn}}\cos(\psi(t)) + C_{\mathrm{y,R}} \quad (19)$$

$$y(t) = \begin{cases} y_{\mathrm{F}}(t), & 0 \leq t \leq t_{\mathrm{FR}} \\ y_{\mathrm{R}}(t), & t_{\mathrm{FR}} < t \leq t_{\mathrm{stop}} \end{cases} \quad (20)$$

The result for both constants to ensure seamlessness is described by Equations (21) and (22).

$$C_{\mathrm{y,F}} = y_0 - \frac{v_0^2\left(z\cos(\psi_0) - 2\sin(\psi_0)\right)}{a_{\mathrm{lon}}(z^2+4)} \quad (21)$$

$$C_{\mathrm{y,R}} = y(t_{\mathrm{FR}}) + r_{\mathrm{turn}}\cos(\psi(t_{\mathrm{FR}})) \quad (22)$$

The trajectory of a braking and turning vehicle is described as $p(t)$, by the compound x- and y-position in Cartesian coordinates over time t.

Before introducing the model extension, we discuss the Basic Model and compare it with the CTRA Model in Section III-B, in order to understand the implications of the approximations and model parameters first.

B. Comparison of Our Basic Model Against CTRA Model

To evaluate the Basic Model's performance with respect to calculation time and to show its correctness, we compare it to a CTRA-Model [19] (*Constant Turn Rate and Acceleration*) in a simulation. The CTRA simulation iteratively moves a vehicle, such that our condition in (1) is fulfilled, and the assumptions introduced in Section II hold. The simulation therefore calculates effectively the same maneuvers as our Basic Model, but in a very different way. We choose the CTRA-Model, as it is well known, allows the vehicle to follow a spiral shape and has the same state space representation as our model. The turn rate and acceleration is assumed to be constant within one of many consecutive time steps Δt.

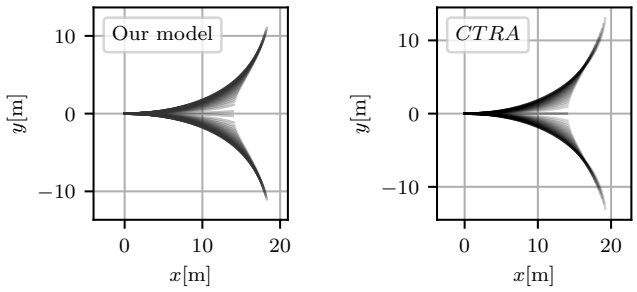

(a) Our basic braking model. (b) CTRA-Model, $\Delta t = 0.0075s$.

Figure 5. Comparison of our Basic Model to the CTRA-Model for 40 vehicle trajectories with linearly sampled b values and equal start state.

The result in Figure 5 shows that our model matches the shape of the CTRA-Model well, without introducing linearization errors as the CTRA-Model does. Both results from Figure 5 show a very similar structure. The starting conditions for both tests are $v_0 = 16.67^{m}/_{s}, \hat{a} = 10^{m}/_{s^2}, r_{\mathrm{turn}} = 12.5m, \psi_0 = 0\ rad$. Note that the CTRA-Model (Figure 5b) has slightly longer trajectories, especially in the outer arms of the structure. This is caused by the CTRA-Model's assumption of a constant turn rate $\dot{\psi}$, which is not correct in this kind of non-linear maneuver. In our model (Figure 5a), the only assumption is that of a constant acceleration, as introduced in Section II.

The main advantage of our model is the fact that we can directly compute certain vehicle positions straight from the formulas derived in Section III-A such that time intensive calculations are not necessary. A comparison of computation times t_{calc} in seconds, and their deviation $\sigma_{t_{\mathrm{calc}}}$ over 10 runs is shown in Table II. In the first test, only the stop states where

computed of 1000 different b values. In the second test, a whole pearl chain of positions from start to stop was computed, with 250 points per b value.

TABLE II. COMPARISON TO THE CTRA MODEL.

Calculate 1000 possible **stop states**, $\Delta t = 0.01112s$						
v_0	5 m/s		10 m/s		20 m/s	
	Mean t_{calc}[s]	$\sigma_{t_{\text{calc}}}$	Mean t_{calc}	$\sigma_{t_{\text{calc}}}$	Mean t_{calc}	$\sigma_{t_{\text{calc}}}$
CTRA	1.0715	0.0137	2.1975	0.0052	4.9310	0.1073
Our model	0.2059	0.0053	0.2078	0.0017	0.2144	0.0075
Calculate 1000 **trajectories**, 250 samples per trajectory, $\Delta t = 0.01112s$						
v_0	5 m/s		10 m/s		20 m/s	
	Mean t_{calc}	$\sigma_{t_{\text{calc}}}$	Mean t_{calc}	$\sigma_{t_{\text{calc}}}$	Mean t_{calc}	$\sigma_{t_{\text{calc}}}$
CTRA	1.0870	0.0207	2.2335	0.0096	4.9761	0.0814
Our model	0.2310	0.0017	0.2326	0.0021	0.2320	0.0011

The table shows that our model is up to 20 times faster in terms of computing time than the CTRA-Model, especially for high initial velocities v_0. This is caused by the fact that CTRA must iteratively compute time steps until the stop position is found, whereas our model can directly compute the stop state.

C. Discussion of Model Uncertainties

In this section, we discuss the effect of individual uncertainties in the model parameters $r_{\text{turn}}, \hat{a}$ and the initial vehicle state $X_0 = [x_0, y_0, v_0, \psi_0]^T$. We model the uncertainties as intervals $\mathcal{I}_\Theta$,$\mathcal{I}_{X_0}$ that contain all possible values. As the parameters are also contained in the Extended Model in Section IV, this discussion is valid for both models.

1) Highest possible deceleration $\hat{a}$: The highest possible deceleration heavily depends on the road and tire conditions, which are often uncertain. The interval $\mathcal{I}_{\hat{a}}$ therefore covers the most slippery and most rough road condition possible. Calculating different stop states X_{stop} with different values for $\hat{a}$ reveals an almost linear behavior within expectable values of $\hat{a} \in \mathcal{I}_{\hat{a}}$.

The resulting shape of 50 different $\hat{a} \in \mathcal{I}_{\hat{a}}$ can be seen in Figure 6a, where lower values of $\hat{a}$ lead to a farther vehicle trajectory with an almost linear behavior. A line segment shows the extending effect of the parameter uncertainties on the top half.

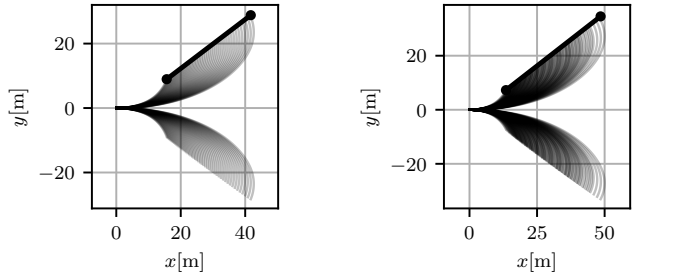

(a) Resulting trajectories at interval $\mathcal{I}_{\hat{a}} = [4, 12]\ \frac{m}{s^2}$.

(b) Resulting trajectories at intervals $\mathcal{I}_{\hat{a}} = [4, 12]\ \frac{m}{s^2}, \mathcal{I}_{v_0} = [15.3, 18.1]\ \frac{m}{s}$

Figure 6. Two sets of trajectories with a b value of -0.6. Left, only considering $\mathcal{I}_{\hat{a}}$. Right, considering $\mathcal{I}_{\hat{a}}$ and $\mathcal{I}_{v_0}$.

2) Smallest possible turning radius r_{turn}: The smallest possible turning radius r_{turn} is a vehicle inherent parameter which influences the trajectory after t_{FR} and also defines the value of t_{FR} itself. Although there are certain legal requirements for r_{turn} depending on vehicle class, the exact value is uncertain, especially when considering other traffic participants.

Any $r_{\text{turn}} \in \mathcal{I}_{r_{\text{turn}}}$ causes a different stopping position. Unfortunately, neither the lowest nor the highest r_{turn} necessarily leads to the outmost stopping position. By observing the stopping positions depending on r_{turn}, one can see that the shape of all stopping positions with different $r_{\text{turn}} \in \mathcal{I}_{r_{\text{turn}}}$ forms a spiral with a rising radius. Let A be the stopping position of the lowest r_{turn}, $A = X_{\text{stop}}|_{r_{\text{turn,min}}}$, and $B = X_{\text{stop}}|_{r_{\text{turn,max}}}$. The circle with radius $r = dist(A, B)$ at center A then includes all points of the spiral, which means all stopping positions can be overestimated by such a circle. By describing this distance as function $d = f(\hat{a}, v_0)$, it can be shown that the maximum distance is at $d_{\max} = f(\hat{a}_{\min}, v_{0,\max})$. Figure 7 shows an example of such a circle.

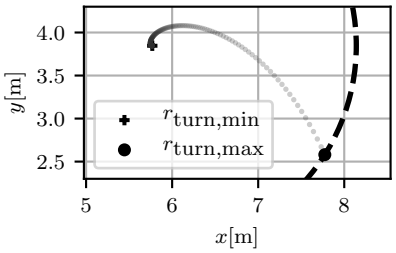

Figure 7. Effect of $\mathcal{I}_{r_{\text{turn}}}$ on X_{stop}. The figure shows how a circle can surround all stopping positions caused by different $r_{\text{turn}} \in \mathcal{I}_{r_{\text{turn}}} = [1\text{e}{-7}, 13]m$.

In order to show the spiral effect in Figure 7, we assumed $\mathcal{I}_{r_{\text{turn}}} = [1\text{e}{-7}, 13]m$ and $v_0 = 10^m/_s$, which results in a circle radius of $\approx 2.4m$. For a more realistic scenario of $\mathcal{I}_{r_{\text{turn}}} = [7, 13]m$ and $v_0 = 10^m/_s$, the radius of the circle is $\approx 1.3m$.

3) Initial velocity v_0: The uncertainty in the initial velocity $\mathcal{I}_{v_0}$ determines the stopping distance similarly to $\mathcal{I}_{\hat{a}}$, as it stretches the possibly reachable positions farther from the start. This means the closest reachable position is defined by $v_{0,\min}$ and $\hat{a}_{\max}$, which stands for a very rough road-to-tire surface. In contrast, the farthest reachable stopping position is defined by the highest velocity $v_{0,\max}$ on the most slippery road $\hat{a}_{\min}$ possible. An example of the resulting shape is shown in Figure 6b.

4) Initial position: The initial position of the vehicle will always be uncertain, as no perfect localization is possible. The effect of an uncertain starting position (x_0, y_0) is however not complex, as a different starting position of $\Delta x, \Delta y$ simply causes a translation of the complete reachable area of $\Delta x, \Delta y$.

5) Initial yaw angle: The initial yaw angle rotates the complete reachable area around the starting position of the vehicle. Figure 8a shows an example of this effect, where $\mathcal{I}_{\psi_0} = [-\pi/32, \pi/32]$.

6) Combination of all uncertainties: So far, we discussed the uncertainty of parameters separately. To describe and overestimate all system states that can potentially be reached under all uncertainties is not in the scope of this paper. In order to do so, a formal reachability analysis must be performed, compare for example [6][8][12][20].

By sampling all parameters from $\mathcal{I}$ and calculating all combinations, we can estimate the reachable area non formally by the union of the resulting shapes.

In Figure 8b we show such a result, where $\mathcal{I}_{\hat{a}} = [7, 11]$, $\mathcal{I}_{r_{\text{turn}}} = [7, 13]$, $\mathcal{I}_{v_0} = [15.3, 18.1]$, $\mathcal{I}_{\psi_0} = [-\pi/32, \pi/32]$, $\mathcal{I}_{x_0} = \mathcal{I}_{y_0} = [-1, 1]$. We sample 3 parameters of each interval. The above section show how the Basic Model of this paper can be used to estimate the Braking Area. To take into account the physics of a limited change rate, we extend the Basic Model by introducing the additional parameters $s, L, \hat{\dot{\delta}}$ and the new model input of $\dot{\psi}_0$ as shown in Figure 3b.

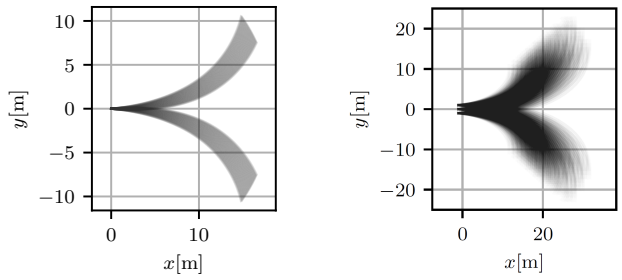

(a) Trajectories at interval $\mathcal{I}_{\psi_0} = [-\pi/32, \pi/32]$. Other parameters, $b = -0.6$, $\hat{a} = 4m/s^2$, $v_0 = 15.3m/s$, $r_{\text{turn}} = 12.5m$.

(b) Trajectories at interval $\mathcal{I}_{\hat{a}} = [7, 11]m/s^2$, $\mathcal{I}_{r_{\text{turn}}} = [7, 13]m$, $\mathcal{I}_{v_0} = [15.3, 18.1]m/s$, $\mathcal{I}_{\psi_0} = [-\pi/32, \pi/32]$rad, $\mathcal{I}_{x_0} = \mathcal{I}_{y_0} = [-1, 1]m$.

Figure 8. The effect of uncertain parameters. Left, only $\mathcal{I}_{\psi_0}$ is considered. Right, all parameters are assumed uncertain.

IV. Extended Model

The missing yaw rate at $t = 0$ permits estimating the reachable area of the vehicle, however, leads to inaccurate trajectory results in situations in which a vehicle has an initial yaw rate $\dot{\psi}_0$ not close or equal to 0, especially when steering is slow.

For the Extended Model, the general positional integrals remain the same as in Equation (3) introduced in the Basic Model. The difference lies in the calculation of yaw angle $\psi(t)$. Instead of directly applying the highest yaw rate permitted by the Friction Circle $\dot{\psi}_{\text{F}}$, we instead start from the current yaw rate at $t = 0$, called $\dot{\psi}_0$. From this point forward, the yaw rate is computed by steering, until the vehicle either reaches its stopping position, or until another limitation is reached.

A. Equations of the Extended Model

This yields three different descriptions of the current yaw rate. In general, the yaw rate is defined in Equation (23) as:

$$\dot{\psi}(t) = \frac{v(t)}{r(t)} = v(t)\kappa(t) \tag{23}$$

where $r(t)$ is the radius of the trajectory and $\kappa(t)$ the respective curvature. An advantage of curvature over radius is that a straight curve has a radius of ∞, but a curvature of 0, which is much easier for computations.

Hence, the difference between the trajectory segments lies in the different descriptions of curvatures, which can be computed trivially.

Figure 9 shows an example of the different curvatures.

In the following, all different curvature types $\kappa_{\text{T}}(t)$, $\kappa_{\text{F}}(t)$ and $\kappa_{\text{R}}(t)$ will be described in detail.

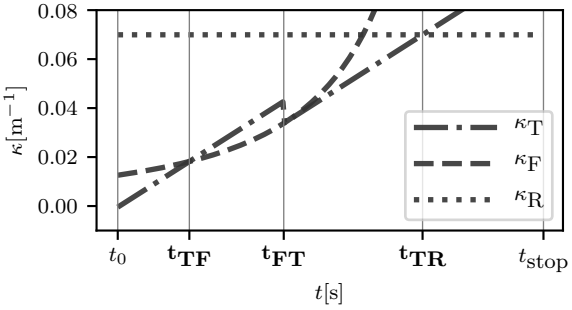

Figure 9. The 3 curvatures $\kappa_{\text{T}}, \kappa_{\text{F}}, \kappa_{\text{R}}$. The minimum of all curves defines the biggest possible curvature in each point in time between $t = 0$ and $t = t_{\text{stop}}$.

Curvature Defined by Change of Steering Angle: The curvature of road vehicles is determined by the steering angle δ, which is set by the steering wheel and is defined by the angle of vehicle longitudinal axis and the direction the wheels are pointing. Because of mechanical and physical limits, the steering wheel cannot be moved arbitrarily fast. To incorporate this property in our Extended Model, we introduce the new parameter $\hat{\dot{\delta}}$, which describes the maximum steering angle change rate. The resulting curvature definition based on the steering angle δ and maximum change rate $\hat{\dot{\delta}}$ is shown in Equation (24):

$$\kappa_{\text{T,l}}(t) = \frac{\delta(t)}{L} = \frac{s\hat{\dot{\delta}}t + \delta_0}{L} \tag{24}$$

where the steering angle at $t = 0$, δ_0, is defined in Equation (25) as:

$$\delta_0 = \frac{\dot{\psi}_0 L}{v_0} \tag{25}$$

However, the description of $\kappa_{\text{T,l}}(t)$ is not sufficient to describe $\kappa_{\text{T}}(t)$ completely. The reason can be seen in Figure 9 in the appearance of κ_{T}, specifically in the jump that the curve performs at t_{FT}. The maximum change rate of steering angle, $\hat{\dot{\delta}}$, not only becomes effective from $t = 0$ onwards, but also at any other times. However, the only situation of such kind, in the model, is when the Friction Circle allows for change in curvature which is greater than $\hat{\dot{\delta}}$. In that case, it must be limited by a differently defined segment of $\kappa_{\text{T}}(t)$, called $\kappa_{\text{T,r}}(t)$. This segment $\kappa_{\text{T,r}}(t)$ is defined as shown in Equation (26), which means that the original curve $\kappa_{\text{T,l}}$ is shifted by an offset o_{T} along the y-axis.

$$\kappa_{\text{T,r}} = \kappa_{\text{T,l}} + o_{\text{T}} \tag{26}$$

The offset o_{T} must ensure that the gradient of $\kappa_{\text{F}}(t)$ does not exceed the gradient of $\kappa_{\text{T}}(t)$. It is defined in Equation (27) as:

$$o_{\text{T}} = \kappa_{\text{F}}(t_{\text{FT}}) - \kappa_{\text{T,l}}(t_{\text{FT}}) \tag{27}$$

where

$$t_{\text{FT}} = -{a_{\text{lon}}}^{-1}\left(\frac{\sqrt[3]{2\hat{a}^2 bL\sqrt{1-b^2}}}{\sqrt[3]{\hat{\dot{\delta}}}} + v_0\right) \tag{28}$$

With this, a complete description of $\kappa_{\text{T}}(t)$ can be formulated as Equation (29):

$$\kappa_{\text{T}}(t) = \min\left(\kappa_{\text{T,l}}(t), \kappa_{\text{T,lr}}(t)\right) \tag{29}$$

where

$$\kappa_{\mathrm{T,lr}}(t) = \begin{cases} \kappa_{\mathrm{T,l}}(t), & 0 \leq t \leq t_{\mathrm{FT}} \\ \kappa_{\mathrm{T,r}}(t), & t_{\mathrm{FT}} < t < t_{\mathrm{stop}} \end{cases} \tag{30}$$

In words, the above Equation (29) means that if $\kappa_{\mathrm{T,l}}$ does not intersect κ_{F}, there is no second segment of κ_{T}. However, if it does intersect, the two-segmented description from Equation (30) shall be used.

The yaw rate based on the initial yaw rate $\dot{\psi}_0$ is hence defined as shown in Equation (31).

$$\dot{\psi}_{\mathrm{T}}(t) = v(t)\kappa_{\mathrm{T}} \tag{31}$$

$\dot{\psi}_{\mathrm{T}}(t)$ describes the yaw rate of a vehicle that is constantly turning as quickly as the mechanical system allows it.

As can be seen in Equation (31), the yaw rate described by constantly changing the steering angle results in a second order polynomial.

If this polynomial was used to further find a description of position, a computationally too expensive intermediate result emerges. The reason for that can be found in $\psi_{\mathrm{T}}(t)$, which naturally is a third order polynomial, see Equation (32).

$$\psi_{\mathrm{T}}(t) = \int \dot{\psi}_{\mathrm{T}}(t)dt = At^3 + Bt^2 + Ct + D \tag{32}$$

where

$$\begin{aligned} A &= \frac{\hat{a}b\hat{\dot{\delta}}s}{3L} \\ B &= \frac{3\hat{a}b\delta_0 + 3\hat{\dot{\delta}}sv_0}{6L} \\ C &= \frac{\delta_0 v_0}{L} \\ D &= \text{const.} \end{aligned}$$

As the position is defined as Equation (33), it means that an integral in the form of $\int t\cos(t^3)dt$ must be solved.

$$p_{\mathrm{T}}(t) = \begin{bmatrix} x_{\mathrm{T}}(t) \\ y_{\mathrm{T}}(t) \end{bmatrix} = \int v(t) \begin{bmatrix} \cos(\psi_{\mathrm{T}}(t)) \\ \sin(\psi_{\mathrm{T}}(t)) \end{bmatrix} dt \tag{33}$$

The integral of Equation (33) leads to a large combination of Incomplete Gamma Functions as described, e.g., by Paris [21, 8]. Though several asymptotic approximations exist, see [21, 8.25], the computational complexity is expected to overrule the resulting gain in accuracy. Hence, we introduce an approximation earlier in the position calculation. Instead of applying the parabolic shape of $\dot{\psi}_{\mathrm{T}}(t)$, we approximate the relevant parabola segment by straight line segments. See the first bold line segment in Figure 10 for an example.

Note that the approximation always under-estimates the actually possible yaw rate and is hence feasible. The formal definition of any approximative line from t_1 to t_2 is shown in Equation (34).

$$\overline{\dot{\psi}_{\mathrm{T}}}(t|t_1, t_2) = \frac{\dot{\psi}(t_2) - \dot{\psi}(t_1)}{t_2 - t_1}\, t + \frac{t_2\dot{\psi}(t_1) - t_1\dot{\psi}(t_2)}{t_2 - t_1} \tag{34}$$

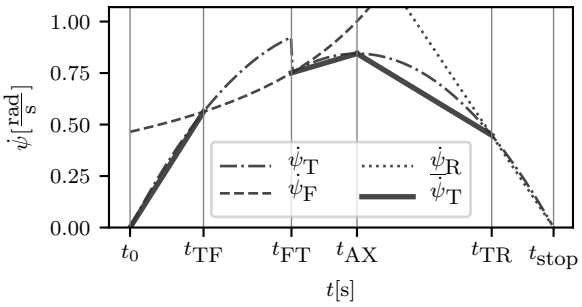

Figure 10. An example of linearizing $\dot{\psi}_{\mathrm{T}}(t)$. Two parabola segments are approximated, the first from 0 to t_{TF}. The second one from t_{FT} to t_{TR}.

where $\dot{\psi}(t_{1,2}) \in \dot{\psi}_{\mathrm{T}}$. Note that even though the chosen yaw rates at $t_{1,2}$ must be $\in \dot{\psi}_{\mathrm{T}}$, they can also be computed with another yaw rate description, as $t_{1,2}$ are intersection times of yaw rates, and hence the yaw rates of at least one other segment of $\dot{\psi}(t)$ are identical at these times.

The second line segment from t_{FT} to t_{TR} in Figure 10 shows a special case that must be considered when linearizing $\dot{\psi}_{\mathrm{T}}$. The parabola segment spans across the parabola's Apex at t_{AX}. See Figure 11 for a more detailed example. If unconsidered, this case could cause large errors.

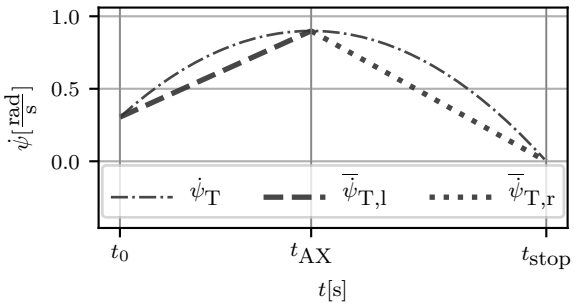

Figure 11. Linearization of $\dot{\psi}_{\mathrm{T}}(t)$ by two line segments $\overline{\dot{\psi}_{\mathrm{T,l}}}$ and $\overline{\dot{\psi}_{\mathrm{T,r}}}$ in the special case that the line segment spans across the Apex Point at time t_{AX}.

The Apex Point is defined in Equation (35), where o_{T} is the offset of the second segment of $\kappa_{\mathrm{T,lr}}$, as introduced in Equation (30).

$$t_{\mathrm{AX}} = -\frac{\hat{a}b\left(\delta_0 + Lo_{\mathrm{T}}\right) + \hat{\dot{\delta}}v_0}{2\hat{a}b\hat{\dot{\delta}}} \tag{35}$$

With these descriptions of approximated yaw rates $\overline{\dot{\psi}_{\mathrm{T}}}$, a resulting description for the yaw angle ψ_{T} can be formulated, now as a second order polynomial as shown in Equation (36).

$$\overline{\psi_{\mathrm{T}}}(t|t_1, t_2) = \frac{\Delta\dot{\psi}}{2\Delta t}t^2 + \frac{\dot{\psi}(t_1)t_2 - \dot{\psi}(t_1)t_1}{\Delta t}t + \psi(t_1) \tag{36}$$

where

$$\begin{aligned} \Delta t &= t_2 - t_1 \\ \Delta\dot{\psi} &= \dot{\psi}(t_2) - \dot{\psi}(t_1) \end{aligned}$$

The compound position Equation (37) is then

$$\begin{aligned}&\overline{p_{\mathrm{T}}}(t|t_1,t_2) = \\ &= \begin{bmatrix} x_{\mathrm{T}}(t) \\ y_{\mathrm{T}}(t) \end{bmatrix} = \int v(t) \begin{bmatrix} \cos(\overline{\psi_{\mathrm{T}}}(t)) \\ \sin(\overline{\psi_{\mathrm{T}}}(t)) \end{bmatrix} dt \\ &= \begin{bmatrix} +\sigma_0 \sin(\xi_0) + \sigma_1(\sin(\xi_1)\mathbb{S} + \cos(\xi_1)\mathbb{C}) \\ -\sigma_0 \cos(\xi_0) + \sigma_1(\cos(\xi_1)\mathbb{S} - \sin(\xi_1)\mathbb{C}) \end{bmatrix} \sigma_2 + C_{\mathrm{p,T}}\end{aligned} \tag{37}$$

where

$$\sigma_1 = \sqrt{\pi \Delta t} \left(\Delta \dot{\psi} v_0 + a_{\mathrm{lon}} \left(\dot{\psi}_2 t_1 - \dot{\psi}_1 t_2 \right) \right)$$

$$\sigma_0 = \sqrt{\Delta \dot{\psi}} a_{\mathrm{lon}} \Delta t \quad \sigma_2 = \Delta \dot{\psi}^{-\frac{3}{2}}$$

$$\xi_0 = \frac{\frac{1}{2}\Delta \dot{\psi} t^2 + \left(\dot{\psi}_1 t_2 - \dot{\psi}_2 t_1 \right) t + \psi_1 t_2 - \dot{\psi}_1 t_1}{\Delta t}$$

$$\xi_1 = \frac{\dot{\psi}_1^2 t_2^2 + \dot{\psi}_2^2 t_1^2 - 2 t_2 \left(\Delta \dot{\psi} \psi_1 + \dot{\psi}_1 \dot{\psi}_2 t_1 \right) + 2 \Delta \dot{\psi} \psi_1 t_1}{2 \Delta \dot{\psi} \Delta t}$$

$$\mathbb{C} = \mathcal{C}(\sigma_3) \quad \mathbb{S} = \mathcal{S}(\sigma_3) \quad \sigma_3 = \frac{\Delta \dot{\psi} t + \dot{\psi}_1 t_2 - \dot{\psi}_2 t_1}{\sqrt{\pi \Delta \dot{\psi} \Delta t}}$$

The constant $C_{\mathrm{p,T}}$ must be calculated specific to the type of trajectory, see Section IV-B for more. Once turning reaches the boundary of the Friction Circle, another set of equations limits the yaw rate and hence defines the yaw angle and the position.

Curvature Defined by Friction Circle: The equations are very similar to the Basic Model, as the Physics are the same. The curvature defined by the Friction Circle is more complex than the linear relation of $\kappa_{\mathrm{T}}(t)$, as can be seen in Equation (38).

$$\kappa_{\mathrm{T}} = s \frac{\hat{a}\sqrt{1-b^2}}{v(t)^2} \tag{38}$$

Note that in addition to the Basic Model, the extended version includes the Steering Direction s. The yaw angle is less complex, as one of the $v(t)$ terms gets removed, see Equation (39).

$$\dot{\psi}_{\mathrm{F}}(t) = s \frac{\hat{a}\sqrt{1-b^2}}{v(t)} \tag{39}$$

Respectively, the yaw angle $\psi_{\mathrm{F}}(t)$ in the Extended Model is shown in Equation (40).

$$\psi_{\mathrm{F}}(t) = sz(\ln(v(t)) - \ln(v_0)) + C_{\dot{\psi},\mathrm{F}} \tag{40}$$

The position calculation is shown in Equation (41):

$$\begin{aligned}p_{\mathrm{F}}(t|t_1) &= \begin{bmatrix} x_{\mathrm{F}}(t) \\ y_{\mathrm{F}}(t) \end{bmatrix} = \int v(t) \begin{bmatrix} \cos(\psi_{\mathrm{F}}(t)) \\ \sin(\psi_{\mathrm{F}}(t)) \end{bmatrix} dt \\ &= \sigma_0 \left[sz \begin{bmatrix} +\sin(\psi_1) \\ -\cos(\psi_1) \end{bmatrix} + 2 \begin{bmatrix} +\cos(\psi_1) \\ -\sin(\psi_1) \end{bmatrix} \right] + C_{\mathrm{p,F}}\end{aligned} \tag{41}$$

where

$$\sigma_0 = v(t)^2 \left(a_{\mathrm{lon}}(z^2 s^2 + 4) \right)^{-1}$$

The constant of integration $C_{\mathrm{p,F}}$ must be adjusted and computed specific to the type of trajectory, see Section IV-B for more. In the Extended Model, the yaw rate can naturally also be limited by the smallest turning radius r_{turn}.

Curvature Defined by Turning Radius: The curvature defined by the turning radius is simply its reciprocal value times s, as shown in Equation (42).

$$\kappa_{\mathrm{R}} = s r_{\mathrm{turn}}^{-1} \tag{42}$$

Note that κ_{R} is independent of time, as it is only defined by properties of the vehicle. The resulting yaw rate is shown in Equation (43):

$$\dot{\psi}_{\mathrm{R}}(t) = s \frac{v(t)}{r_{\mathrm{turn}}} \tag{43}$$

The yaw angle is shown in Equation (44):

$$r_{\mathrm{turn}}^{-1} \left(\frac{1}{2} s a_{\mathrm{lon}} t^2 + s v_0 t \right) + C_{\psi,\mathrm{R}} \tag{44}$$

The resulting position defined by the turning radius in the Extended Model is shown in Equation (45):

$$\begin{aligned}p_{\mathrm{R}}(t|t_1) &= \begin{bmatrix} x_{\mathrm{R}}(t) \\ y_{\mathrm{R}}(t) \end{bmatrix} = \int v(t) \begin{bmatrix} \cos(\psi_{\mathrm{R}}(t)) \\ \sin(\psi_{\mathrm{R}}(t)) \end{bmatrix} dt \\ &= s r_{\mathrm{turn}} \begin{bmatrix} +\sin(\psi_1) \\ -\cos(\psi_1) \end{bmatrix} + C_{\mathrm{p,R}}\end{aligned} \tag{45}$$

In order to calculate trajectories, the different position descriptions must be interconnected to ensure seamlessness in terms of angle and position. This is done by appropriately choosing the constants of integration of all position and yaw angle equations. For that purpose, the intersection times of all curvatures play a major role. In the Basic Model, the intersection time is defined easily because there is only one. In contrast, the Extended Model has different intersection times, and their calculation is partially less trivial.

The Meaning of Curvature Intersections: The curvature of a resulting trajectory is limited by the three curves $\kappa_{\mathrm{T}}(t), \kappa_{\mathrm{F}}(t), \kappa_{\mathrm{R}}(t)$. For positive curvatures, as shown in Figure 9, the maximally curved trajectory considering all inputs is hence defined as shown in Equations (46) and (47).

$$\kappa(t) = \min(\kappa_{\mathrm{T}}(t), \kappa_{\mathrm{F}}(t), \kappa_{\mathrm{R}}) \forall t \in [0, t_{\mathrm{stop}}] \tag{46}$$

$$\dot{\psi}(t) = \min(\dot{\psi}_{\mathrm{T}}(t), \dot{\psi}_{\mathrm{F}}(t), \dot{\psi}_{\mathrm{R}}(t)) \forall t \in [0, t_{\mathrm{stop}}] \tag{47}$$

The yaw rate curves intersect at the same times as the curvatures, as long as $v(t) \neq 0$, because

$$\begin{aligned}\dot{\psi}_x &= \dot{\psi}_y && \Leftrightarrow \\ v(t)\kappa_x &= v(t)\kappa_y && \Leftrightarrow \\ \kappa_x &= \kappa_y && \forall v(t) \neq 0 \Leftrightarrow \forall t \neq t_{\mathrm{stop}}\end{aligned}$$

Therefore, the different sections of the Extended Model trajectory are each limited by the respective intersection times of the three curvatures. The intersection at t_{stop} is not relevant for that, as the model ends its calculations when velocity is 0. An overview of all yaw rates is given in Figure 12, which shows all different characteristics that describe the course of the yaw rates of a vehicle while braking and turning.

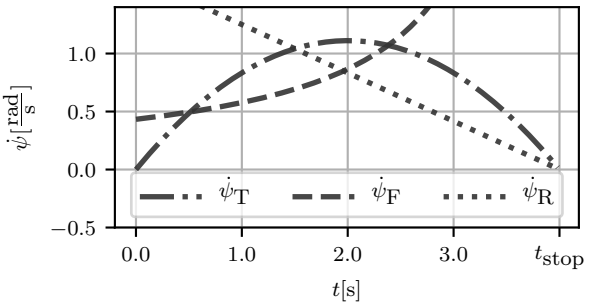

Figure 12. The 3 different yaw rate characteristics $\dot{\psi}_\text{T}$, $\dot{\psi}_\text{F}$, $\dot{\psi}_\text{R}$. The Extended Model assumes the minimum of all yaw rates at each point in time.

All yaw rate descriptions have in common that they describe the maximal yaw rate possible. That means that at all times t, the yaw rate is limited by all three descriptions.

As shown in the Basic Model, the yaw angle $\psi(t)$ is the integral over the yaw rate $\dot{\psi}(t)$ over time. In order to integrate $\dot{\psi}(t)$, a step wise definition is helpful, similar to Equation (5) of the Basic Model. We thus define $\dot{\psi}(t)$ as shown in Equation (48).

$$\dot{\psi}(t) = \begin{cases} \dot{\psi}_\text{T}(t), & 0 \leq t \leq t_\text{TF} \\ \dot{\psi}_\text{F}(t), & t_\text{TF} < t \leq t_\text{FR} \\ \dot{\psi}_\text{R}(t), & t_\text{FR} < t < t_\text{stop} \end{cases}, \forall t \geq 0 \tag{48}$$

where

$$\dot{\psi}_\text{T}(t) = v(t)(s\hat{\dot{\delta}}t + \delta_0)L^{-1} \tag{49}$$

$$\dot{\psi}_\text{F}(t) = s\hat{a}\sqrt{1-b^2}\ v^{-1}(t) \tag{50}$$

$$\dot{\psi}_\text{R}(t) = sv(t)r_\text{turn}^{-1} \tag{51}$$

where s is the direction of steering and only defines a positive or negative sign, positive meaning *turning left* and negative *turning right*.

From Figure 12 and Equation (48) follows that the model behavior is defined by the positions of intersections of the different yaw rate descriptions, and all limit the vehicle movement in their own way. Therefore, the definition of these times is very important. Simply put, these times are the times at which the different curvatures intersect.

The intersections of κ_T and $\kappa_\text{F} \in \mathbb{R}$ can be found by applying Cardano's formula [22] to the Cubic Equation (52):

$$At^3 + Bt^2 + Ct + D = 0 \tag{52}$$

where

$$A = s{a_\text{lon}}^2\hat{\dot{\delta}} \tag{53}$$

$$B = {a_\text{lon}}^2\delta_0 + 2sa_\text{lon}v_0\hat{\dot{\delta}} \tag{54}$$

$$C = 2a_\text{lon}v_0\delta_0 + s\hat{\dot{\delta}}{v_0}^2 \tag{55}$$

$$D = \delta_0{v_0}^2 - sL\hat{a}\sqrt{1-b^2} \tag{56}$$

The determinant is defined as Equation (57):

$$\Delta := \left(\frac{q}{2}\right)^2 + \left(\frac{p}{3}\right)^3 \tag{57}$$

where

$$p = \beta - \frac{\alpha^2}{3} \tag{58}$$

$$q = \frac{2\alpha^3}{27} - \frac{\alpha\beta}{3} + \gamma \tag{59}$$

$$u = \sqrt[3]{-\frac{q}{2} + \sqrt{\Delta}} \tag{60}$$

$$v = \sqrt[3]{-\frac{q}{2} - \sqrt{\Delta}} \tag{61}$$

with $\alpha = {}^A\!/_D$, $\beta = {}^B\!/_D$ and $\gamma = {}^C\!/_D$.

If $\Delta > 0$, there is only one intersection $\in \mathbb{R}$ at

$$t_\text{T,F,0} = u + v - \frac{B}{3A} \tag{62}$$

If $\Delta = 0$ and $p = 0$, there is a triple intersection $\in \mathbb{R}$ at

$$t_\text{T,F,0,1,2} = -\frac{B}{3A} \tag{63}$$

If $\Delta = 0$ but $p \neq 0$, there are three solutions $\in \mathbb{R}$ at

$$t_\text{T,F,0} = \frac{3q}{p} - \frac{B}{3A} \tag{64}$$

$$t_\text{T,F,1,2} = -\frac{3q}{2p} - \frac{B}{3A} \tag{65}$$

If $\Delta < 0$, there are also three solutions $\in \mathbb{R}$, which may be calculated by

$$t_\text{T,F,0} = \sqrt{-\frac{4}{3}p}\cos\left(\sigma_\text{T,F}\right) - \frac{B}{3A} \tag{66}$$

$$t_\text{T,F,1} = \sqrt{-\frac{4}{3}p}\cos\left(\sigma_\text{T,F} + \frac{\pi}{3}\right) - \frac{B}{3A} \tag{67}$$

$$t_\text{T,F,2} = \sqrt{-\frac{4}{3}p}\cos\left(\sigma_\text{T,F} - \frac{\pi}{3}\right) - \frac{B}{3A} \tag{68}$$

where

$$\sigma_\text{T,F} = \frac{1}{3}\arccos\left(-\frac{q}{2}\sqrt{-\frac{27}{p^3}}\right)$$

The other intersection times can be calculated generally as:

$$t_\text{F,R,0} = -\frac{v_0 + \sqrt{\hat{a}r_\text{turn}\sqrt{1-b^2}}}{a_\text{lon}} \tag{69}$$

$$t_\text{F,R,1} = -\frac{v_0 - \sqrt{\hat{a}r_\text{turn}\sqrt{1-b^2}}}{a_\text{lon}} \tag{70}$$

$$t_\text{T,R,0} = -\frac{v_0}{a_\text{lon}} = t_\text{stop} \tag{71}$$

$$t_\text{T,R,1} = -\frac{sL + \delta_0 r_\text{turn}}{\hat{s\dot{\delta}}r_\text{turn}} \tag{72}$$

Equations (62) to (72) describe all possible intersection times between the different yaw rate limits. Because the curvature defined by the Friction Circle κ_F is strictly increasing or decreasing in $[0, t_\text{stop}]$ (depending on s), the linear function $\kappa_\text{F}(t)$ intersects $\kappa_\text{T}(t)$ possibly at two times in the interval $[0, t_\text{stop}]$. Also, note that $\dot{\psi}_\text{T}$ intersects $\dot{\psi}_\text{R}$ also in t_stop, even though the curvatures are not equal, because the equality condition only holds for $v(t) \neq 0$, which however is the case at t_stop. See Figure 12 for an example.

B. Different Trajectory Types of the Extended Model

As shown above, the positions of yaw rate intersection define the course of a trajectory. An intersection time is called *relevant*, when at this time, the calculation changes from one of the yaw rate description of $\dot{\psi}_{\mathrm{T}}(t)$, $\dot{\psi}_{\mathrm{F}}(t)$, $\dot{\psi}_{\mathrm{R}}(t)$ to another one.

In Figure 13, all intersection times are shown. The relevant times for this example are written in bold.

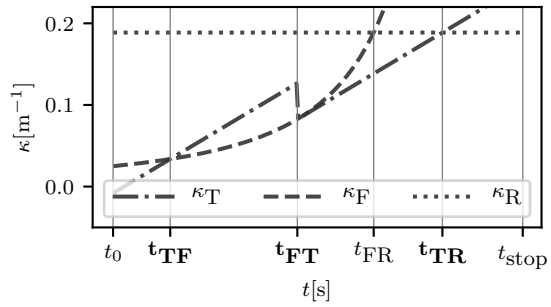

Figure 13. An example of relevant curvature intersections. All relevant intersections are marked in bold.

Depending on the input parameters, different types of trajectories evolve. In this paper, we distinguish between 9 different types. In Figure 14, we show all possible sub-elements of a trajectory and interpret the calculation of a trajectory as one of 9 different possible combinations of subsequent state changes.

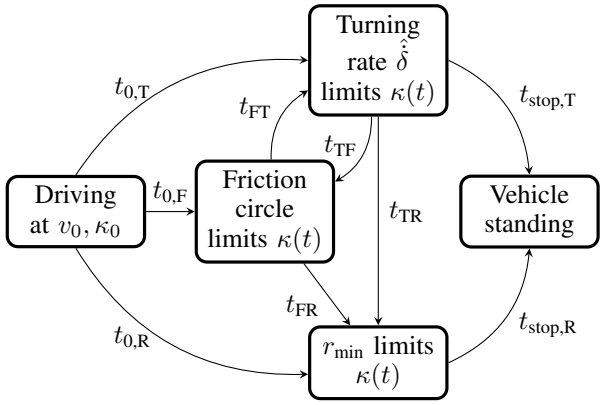

Figure 14. State diagram of all possible sub-elements of a trajectory. State changes occurs at intersections of curvatures and at t_0 and t_{stop}

Figure 14 shows which intersection times are relevant in each state. It also serves as a reference to find all possible combinations of states, and therefore all trajectory types that follow from the Extended Model.

Trajectory Type A: The state changes for Type A Trajectories are defined by the sequence $t_{0,\mathrm{T}} \to t_{\mathrm{TF}} \to t_{\mathrm{FR}} \to t_{\mathrm{stop,R}}$ in Figure 14.

Figure 15 shows the yaw rates of a Type A Trajectory. The effective yaw rate is always defined by the *minimum of all yaw rates* when turning left ($s = +$). This is marked by a thick line.

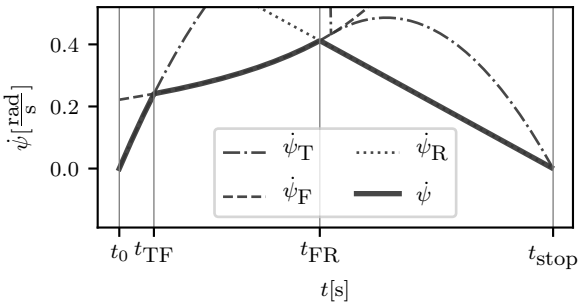

Figure 15. The yaw rates of a Type A trajectory. The effective yaw rate is marked by a thick line style.

The yaw angle function for all Type A trajectories is defined as Equation (73):

$$\psi(t) = \begin{cases} \overline{\psi_{\mathrm{T}}}(t) = \widetilde{\overline{\psi_{\mathrm{T}}}}(t) + C_{\psi,T}, & 0 \le t \le t_{\mathrm{TF}} \\ \psi_{\mathrm{F}}(t) = \widetilde{\psi_{\mathrm{F}}}(t) + C_{\psi,F}, & t_{\mathrm{TF}} < t \le t_{\mathrm{FR}} \\ \psi_{\mathrm{R}}(t) = \widetilde{\psi_{\mathrm{R}}}(t) + C_{\psi,R}, & t_{\mathrm{FR}} < t < t_{\mathrm{stop}} \end{cases} \tag{73}$$

where the constants of integration must be chosen specific to this trajectory type as shown in Equations (74) to (76):

$$C_{\psi,T} = \psi_0 \tag{74}$$

$$C_{\psi,F} = \overline{\psi_{\mathrm{T}}}(t_{\mathrm{TF}}) - \widetilde{\psi_{\mathrm{F}}}(t_{\mathrm{TF}}) \tag{75}$$

$$C_{\psi,R} = \psi_{\mathrm{F}}(t_{\mathrm{FR}}) - \widetilde{\psi_{\mathrm{R}}}(t_{\mathrm{FR}}) \tag{76}$$

The constants for $\Psi(t)$ are chosen in a way that all trajectory segments continue seamlessly.

The positions are calculated respectively in the same time intervals as in Equation (77):

$$p(t) = \begin{cases} p_{\mathrm{T}}(t) = \widetilde{p_{\mathrm{T}}}(t) + C_{\mathrm{p,T}}, & 0 \le t \le t_{\mathrm{TF}} \\ p_{\mathrm{F}}(t) = \widetilde{p_{\mathrm{F}}}(t) + C_{\mathrm{p,F}}, & t_{\mathrm{TF}} < t \le t_{\mathrm{FR}} \\ p_{\mathrm{R}}(t) = \widetilde{p_{\mathrm{R}}}(t) + C_{\mathrm{p,R}}, & t_{\mathrm{FR}} < t < t_{\mathrm{stop}} \end{cases} \tag{77}$$

where the constants of integration must be chosen in a way that all trajectory segments fit together seamlessly, as noted in Equations (78) to (80):

$$C_{p,T} = p_0 - \widetilde{p_{\mathrm{T}}}(0) \tag{78}$$

$$C_{p,F} = p_{\mathrm{T}}(t_{\mathrm{TF}}) - \widetilde{p_{\mathrm{F}}}(t_{\mathrm{TF}}) \tag{79}$$

$$C_{p,R} = p_{\mathrm{R}}(t_{\mathrm{FR}}) - \widetilde{p_{\mathrm{R}}}(t_{\mathrm{FR}}) \tag{80}$$

See Figure 16a for a set of different Type A Trajectories. The model parameters and inputs are equal in all examples of Type A, except for the Braking Factor b, which is chosen to be in an admissible range to result in Type A Trajectories. Note that these trajectories are parametrized in a way that demonstrates the differences well.

Trajectory Type B: These trajectories are the most complex ones that can be described by the Extended Model, as it has the most different segment types. Examples are shown in Figure 16b. The resulting yaw rate segments are defined by the state change sequence $t_{0,\mathrm{T}} \to t_{\mathrm{TF}} \to t_{\mathrm{FT}} \to t_{\mathrm{TR}} \to t_{\mathrm{stop,R}}$ in Figure 14. Figure 17 shows the yaw rates of a Type B Trajectory, where the effective yaw rate is marked by a thick line.

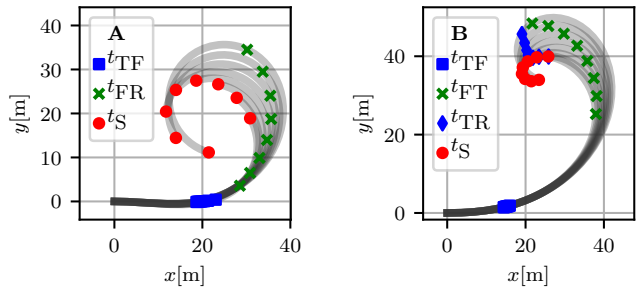

(a) Eight Type A Trajectories. (b) Eight Type B Trajectories.

Figure 16. Type A and Type B trajectories. Both types are shown in rather theoretic situations for demonstration purposes.

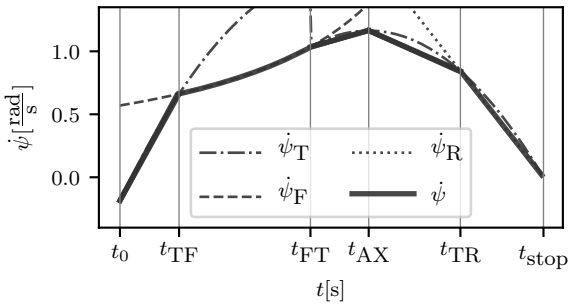

Figure 17. The yaw rates of a Type B trajectory. The five effective yaw rate segments are drawn bold, including the Apex Point of $\dot{\psi}_T$.

The yaw angle function for all Type B trajectories is defined as Equation (81):

$$\psi(t) = \begin{cases} \overline{\psi_{T,0}}(t) = \widetilde{\overline{\psi_T}}(t) + C_{\psi,T,0}, & 0 \le t \le t_{TF} \\ \psi_F(t) = \widetilde{\psi_F}(t) + C_{\psi,F}, & t_{TF} < t \le t_{FT} \\ \overline{\psi_{T,1}}(t) = \widetilde{\overline{\psi_T}}(t) + C_{\psi,T,1}, & t_{FT} < t \le t_{TR} \\ \psi_R(t) = \widetilde{\psi_R}(t) + C_{\psi,R}, & t_{TR} < t < t_{stop} \end{cases} \quad (81)$$

where the constants of integration must be chosen specific to this trajectory type as shown in Equations (82) to (85):

$$C_{\psi,T,0} = \psi_0 \quad (82)$$
$$C_{\psi,F} = \overline{\psi_T}(t_{TF}) - \widetilde{\psi_F}(t_{TF}) \quad (83)$$
$$C_{\psi,T,1} = \psi_F(t_{FT}) - \widetilde{\overline{\psi_T}}(t_{FT}) \quad (84)$$
$$C_{\psi,R} = \overline{\psi_T}(t_{TR}) - \widetilde{\psi_R}(t_{TR}) \quad (85)$$

The constants for $\Psi(t)$ are chosen in a way that all trajectory segments continue seamlessly.

The positions are calculated respectively in the same time intervals as in Equation (77):

$$p(t) = \begin{cases} p_{T,0}(t) = \widetilde{p_T}(t) + C_{p,T,0}, & 0 \le t \le t_{TF} \\ p_F(t) = \widetilde{p_F}(t) + C_{p,F}, & t_{TF} < t \le t_{FT} \\ p_{T,1}(t) = \widetilde{p_T}(t) + C_{p,T,1}, & t_{FT} < t \le t_{TR} \\ p_R(t) = \widetilde{p_R}(t) + C_{p,R}, & t_{TR} < t < t_{stop} \end{cases} \quad (86)$$

where the constants of integration must be chosen in a way that all trajectory segments fit together seamlessly, as noted in Equations (87) to (90):

$$C_{p,T,0} = p_0 - \widetilde{p_T}(0) \quad (87)$$
$$C_{p,F} = p_{T,0}(t_{TF}) - \widetilde{p_F}(t_{TF}) \quad (88)$$
$$C_{p,T,1} = p_F(t_{FT}) - \widetilde{p_{T,1}}(t_{FT}) \quad (89)$$
$$C_{p,R} = p_{T,1}(t_{TR}) - \widetilde{p_R}(t_{TR}) \quad (90)$$

See Figure 16b for a set of different Type B Trajectories. The model parameters and inputs are equal in all examples of Type B, except for the Braking Factor b, which is chosen to be in an admissible range to result in Type B Trajectories.

Trajectory Type C: The state changes for Type C Trajectories are defined by the sequence $t_{0,T} \rightarrow t_{TR} \rightarrow t_{stop,R}$ in Figure 14.
Figure 18 shows the yaw rates of a Type C Trajectory. The effective yaw rate is marked by a thick line.

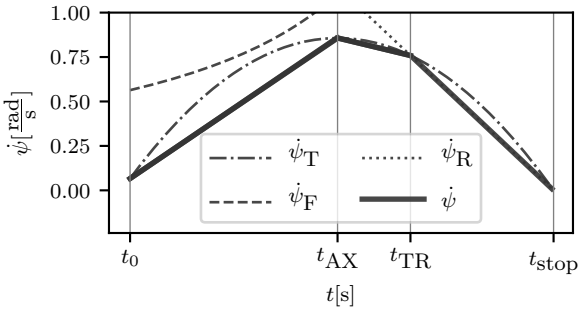

Figure 18. The yaw rates of a Type C trajectory. The effective yaw rate is marked by a thick line style.

The yaw angle function for all Type C trajectories is defined as Equation (91):

$$\psi(t) = \begin{cases} \overline{\psi_T}(t) = \widetilde{\overline{\psi_T}}(t) + C_{\psi,T}, & 0 \le t \le t_{TR} \\ \psi_R(t) = \widetilde{\psi_R}(t) + C_{\psi,R}, & t_{TR} < t < t_{stop} \end{cases} \quad (91)$$

where the constants of integration must be chosen specific to this trajectory type as shown in Equations (92) and (93):

$$C_{\psi,T} = \psi_0 \quad (92)$$
$$C_{\psi,R} = \psi_T(t_{TR}) - \widetilde{\psi_R}(t_{TR}) \quad (93)$$

The constants for $\Psi(t)$ are chosen in a way that all trajectory segments continue seamlessly.

The positions are calculated respectively in the same time intervals as in Equation (94):

$$p(t) = \begin{cases} p_T(t) = \widetilde{p_T}(t) + C_{p,T}, & 0 \le t \le t_{TR} \\ p_R(t) = \widetilde{p_R}(t) + C_{p,R}, & t_{TR} < t < t_{stop} \end{cases} \quad (94)$$

where the constants of integration must be chosen in a way that all trajectory segments fit together seamlessly, as noted in Equations (95) and (96):

$$C_{p,T} = p_0 - \widetilde{p_T}(0) \quad (95)$$
$$C_{p,R} = p_R(t_{TR}) - \widetilde{p_R}(t_{TR}) \quad (96)$$

See Figure 19a for a set of different Type C Trajectories. The model parameters and inputs are equal in all examples of Type C, except for the Braking Factor b, which is chosen to be in an admissible range to result in Type C Trajectories. It can be seen that all trajectories are on top of each other, which

makes sense, because the braking factor only has influence on the actual direction when the Friction Circle is involved in the calculation. In Type C trajectories, this is not the case.

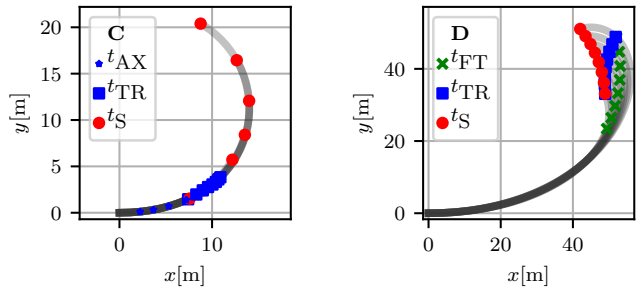

(a) Eight Type C Trajectories. (b) Eight Type D Trajectories.

Figure 19. Different trajectories of both Type C and Type D.

Trajectory Type D: The state changes for Type D Trajectories are defined by the sequence $t_{0,F} \rightarrow t_{FT} \rightarrow t_{TR} \rightarrow t_{stop,R}$ in Figure 14. Hence, Type D Trajectories are like Type B but are limited by the Friction Circle from the beginning on.

Figure 20 shows the yaw rates of a Type D Trajectory. The effective yaw rate is always defined by the *minimum of all yaw rates* when turning left ($s = +$). This is marked by a thick line in Figure 20.

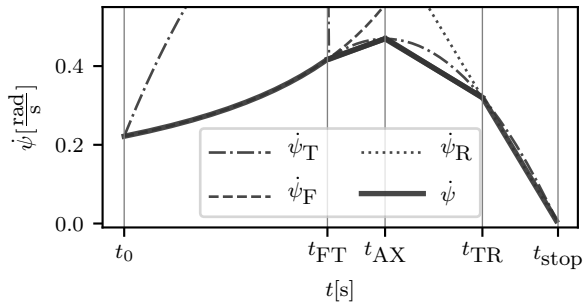

Figure 20. The yaw rates of a Type D trajectory. The effective yaw rate is marked by a thick line style.

The yaw angle function for all Type D trajectories is defined as Equation (97):

$$\psi(t) = \begin{cases} \psi_F(t) = \widetilde{\psi_F}(t) + C_{\psi,F}, & 0 < t \leq t_{FT} \\ \widetilde{\psi_T}(t) = \widetilde{\psi_T}(t) + C_{\psi,T}, & t_{FT} < t \leq t_{TR} \\ \psi_R(t) = \widetilde{\psi_R}(t) + C_{\psi,R}, & t_{TR} < t < t_{stop} \end{cases} \quad (97)$$

where the constants of integration must be chosen specific to this trajectory type as shown in Equations (98) to (100):

$$C_{\psi,F} = \psi_0 \quad (98)$$
$$C_{\psi,T} = \psi_F(t_{TF}) - \widetilde{\psi_F}(t_{TF}) \quad (99)$$
$$C_{\psi,R} = \psi_T(t_{TR}) - \widetilde{\psi_R}(t_{TR}) \quad (100)$$

The constants for $\Psi(t)$ are chosen in a way that all trajectory segments continue seamlessly.

The positions are calculated respectively in the same time intervals as in Equation (101):

$$p(t) = \begin{cases} p_F(t) = \widetilde{p_F}(t) + C_{p,F}, & 0 \leq t \leq t_{FT} \\ p_T(t) = \widetilde{p_T}(t) + C_{p,T}, & t_{FT} < t \leq t_{TR} \\ p_R(t) = \widetilde{p_R}(t) + C_{p,R}, & t_{TR} < t < t_{stop} \end{cases} \quad (101)$$

where the constants of integration must be chosen in a way that all trajectory segments fit together seamlessly, as noted in Equations (102) to (104):

$$C_{p,F} = p_0 - \widetilde{p_F}(0) \quad (102)$$
$$C_{p,T} = p_T(t_{FT}) - \widetilde{p_T}(t_{FT}) \quad (103)$$
$$C_{p,R} = p_R(t_{TR}) - \widetilde{p_R}(t_{TR}) \quad (104)$$

See Figure 19b for a set of different Type D Trajectories. The model parameters and inputs are equal in all examples of Type D, except for the Braking Factor b, which is chosen to be in an admissible range to result in Type D Trajectories.

Trajectory Type E: The state changes for Type E Trajectories are defined by the sequence $t_{0,F} \rightarrow t_{FR} \rightarrow t_{stop,R}$ in Figure 14.

Figure 21 shows the yaw rates of a Type E Trajectory. The effective yaw rate is marked by a thick line.

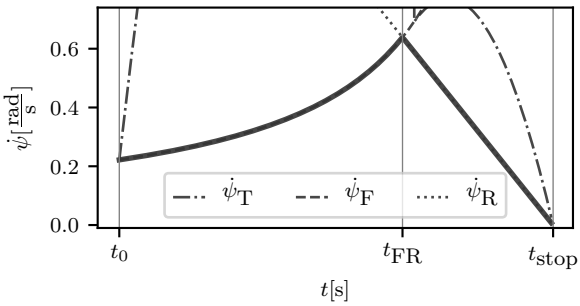

Figure 21. The yaw rates of a Type E trajectory. The effective yaw rate is marked by a thick line style.

The yaw angle function for all Type E trajectories is defined as Equation (105):

$$\psi(t) = \begin{cases} \psi_F(t) = \widetilde{\psi_F}(t) + C_{\psi,F}, & 0 \leq t \leq t_{FR} \\ \psi_R(t) = \widetilde{\psi_R}(t) + C_{\psi,R}, & t_{FR} < t < t_{stop} \end{cases} \quad (105)$$

where the constants of integration must be chosen specific to this trajectory type as shown in Equations (106) and (107):

$$C_{\psi,F} = \psi_0 \quad (106)$$
$$C_{\psi,R} = \psi_F(t_{FR}) - \widetilde{\psi_R}(t_{FR}) \quad (107)$$

The constants for $\Psi(t)$ are chosen in a way that all trajectory segments continue seamlessly.

The positions are calculated respectively in the same time intervals as in Equation (108):

$$p(t) = \begin{cases} p_F(t) = \widetilde{p_F}(t) + C_{p,F}, & 0 \leq t \leq t_{FR} \\ p_R(t) = \widetilde{p_R}(t) + C_{p,R}, & t_{FR} < t < t_{stop} \end{cases} \quad (108)$$

where the constants of integration must be chosen in a way that all trajectory segments fit together seamlessly, as noted in Equations (109) and (110):

$$C_{p,F} = p_0 - \widetilde{p_F}(0) \quad (109)$$
$$C_{p,R} = p_R(t_{FR}) - \widetilde{p_R}(t_{FR}) \quad (110)$$

See Figure 22a for a set of different Type E Trajectories. The model parameters and inputs are equal in all examples of Type E, except for the Braking Factor b, which is chosen to be in an admissible range to result in Type E Trajectories.

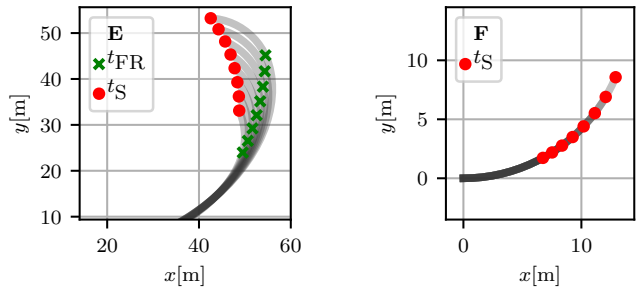

(a) Eight Type E Trajectories. (b) Eight Type F Trajectories.

Figure 22. Different trajectories of both Type E and Type F.

Trajectory Type F: The state changes for Type F Trajectories are defined by the simple sequence $t_{0,R} \rightarrow t_{stop,R}$ in Figure 14. Figure 23 shows the yaw rate of a Type F Trajectory. The effective yaw rate is marked by a thick line to underline the simplicity of Type F trajectories.

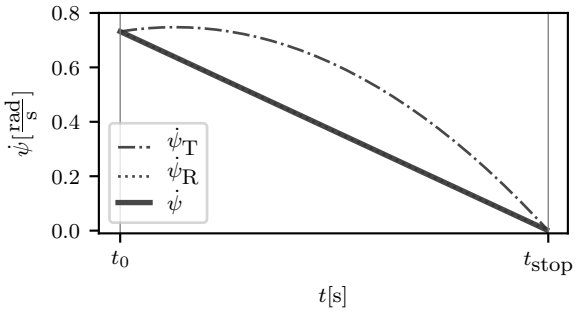

Figure 23. The yaw rates of a Type F trajectory. The effective yaw rate is drawn bold. Note that in this Type $\dot{\psi}$ and $\dot{\psi}_R$ are identical.

The yaw angle function for all Type F trajectories is defined as Equation (111):

$$\psi(t) = \psi_R(t) = \widetilde{\psi_R}(t) + C_{\psi,R}, \quad t_0 \leq t < t_{stop} \tag{111}$$

where the constant of integration must be chosen specific to this trajectory type as shown in Equation (112):

$$C_{\psi,R} = \psi_0 - \widetilde{\psi_R}(t_0) \tag{112}$$

The constant for $\Psi(t)$ is chosen in a way that the trajectory starts correctly with ψ_0.

The positions are calculated respectively in the same time intervals as in Equation (113):

$$p(t) = p_R(t) = \widetilde{p_R}(t) + C_{p,R}, \quad t_0 \leq t < t_{stop} \tag{113}$$

where the constant of integration must be chosen in a way that the trajectory starts correctly at p_0, as noted in Equation (114):

$$C_{p,R} = p_0 - \widetilde{p_R}(t_0) \tag{114}$$

See Figure 22b for a set of different Type F Trajectories. The model parameters and inputs are equal in all examples of Type F, except for the Braking Factor b, which is chosen to be in an admissible range to result in Type F Trajectories. It can be seen that all trajectories are on top of each other, which makes sense, because the braking factor only has influence on the actual direction when the Friction Circle is involved in the calculation. In Type F trajectories this is not the case.

Trajectory Type G: Type G Trajectories are similar to Type B Trajectories, but in contrast they end before reaching r_{turn}. The segments are defined by the state change sequence $t_{0,T} \rightarrow t_{TF} \rightarrow t_{FT} \rightarrow t_{stop,T}$ in Figure 14. Figure 24 shows the yaw rates of a Type G Trajectory. The effective yaw rate is marked by a thick line in Figure 24.

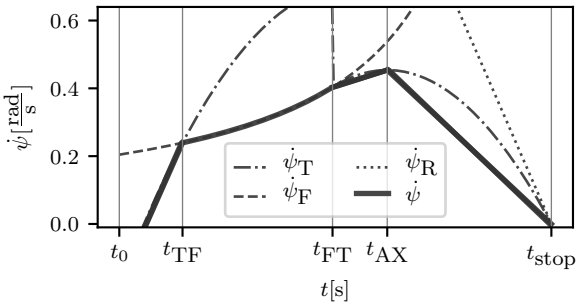

Figure 24. The yaw rates of a Type G trajectory. The effective yaw rate is marked by a thick line style.

The yaw angle function for all Type G trajectories is defined as Equation (115):

$$\psi(t) = \begin{cases} \overline{\psi_{T,0}}(t) = \widetilde{\psi_T}(t) + C_{\psi,T,0}, & 0 \leq t \leq t_{TF} \\ \psi_F(t) = \widetilde{\psi_F}(t) + C_{\psi,F}, & t_{TF} < t \leq t_{FT} \\ \overline{\psi_{T,1}}(t) = \widetilde{\psi_T}(t) + C_{\psi,T,1}, & t_{FT} < t \leq t_{stop} \end{cases} \tag{115}$$

where the constants of integration must be chosen specific to this trajectory type as shown in Equations (116) to (118):

$$C_{\psi,T,0} = \psi_0 \tag{116}$$

$$C_{\psi,F} = \overline{\psi_T}(t_{TF}) - \widetilde{\psi_F}(t_{TF}) \tag{117}$$

$$C_{\psi,T,1} = \psi_F(t_{FT}) - \widetilde{\overline{\psi_T}}(t_{FT}) \tag{118}$$

The constants for $\Psi(t)$ are chosen in a way that all trajectory segments continue seamlessly.

The positions are calculated respectively in the same time intervals as in Equation (119):

$$p(t) = \begin{cases} p_{T,0}(t) = \widetilde{p_T}(t) + C_{p,T,0}, & 0 \leq t \leq t_{TF} \\ p_F(t) = \widetilde{p_F}(t) + C_{p,F}, & t_{TF} < t \leq t_{FT} \\ p_{T,1}(t) = \widetilde{p_T}(t) + C_{p,T,1}, & t_{FT} < t \leq t_{stop} \end{cases} \tag{119}$$

where the constants of integration must be chosen in a way that all trajectory segments fit together seamlessly, as noted in Equations (120) to (122):

$$C_{p,T,0} = p_0 - \widetilde{p_T}(0) \tag{120}$$

$$C_{p,F} = p_{T,0}(t_{TF}) - \widetilde{p_F}(t_{TF}) \tag{121}$$

$$C_{p,T,1} = p_F(t_{FT}) - \widetilde{p_{T,1}}(t_{FT}) \tag{122}$$

See Figure 25a for a set of different Type G Trajectories. The model parameters and inputs are equal in all examples of Type G, except for the Braking Factor b, which is chosen to be in an admissible range to result in Type G Trajectories.

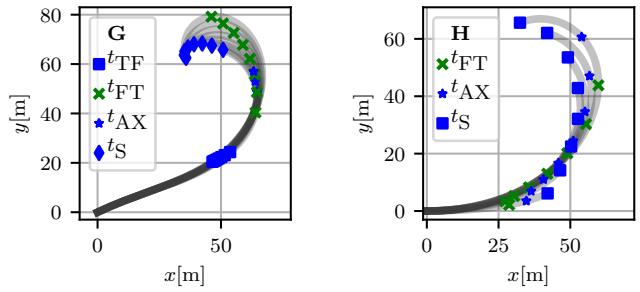

(a) Eight Type G Trajectories. (b) Eight Type H Trajectories.

Figure 25. Different trajectories of both Type G and Type H.

Trajectory Type H: The state changes for Type H Trajectories are defined by the sequence $t_{0,F} \rightarrow t_{FT} \rightarrow t_{stop,R}$ in Figure 14.

Figure 26 shows the yaw rates of a Type H Trajectory. The effective yaw rate is marked by a thick line.

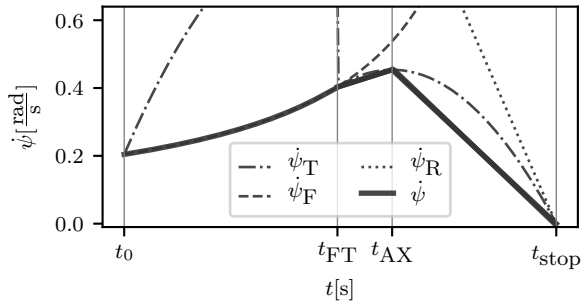

Figure 26. The yaw rates of a Type H trajectory. The effective yaw rate is drawn bold. Notice the similarity to Type G Trajectories as shown in Figure 24

The yaw angle function for all Type H trajectories is defined as Equation (123):

$$\psi(t) = \begin{cases} \psi_F(t) = \widetilde{\psi_F}(t) + C_{\psi,F}, & 0 \le t \le t_{FT} \\ \psi_T(t) = \widetilde{\psi_T}(t) + C_{\psi,T}, & t_{FT} < t < t_{stop} \end{cases} \quad (123)$$

where the constants of integration must be chosen specific to this trajectory type as shown in Equations (124) and (125):

$$C_{\psi,F} = \psi_0 \quad (124)$$

$$C_{\psi,T} = \psi_F(t_{FT}) - \widetilde{\psi_R}(t_{FT}) \quad (125)$$

The constants for $\Psi(t)$ are chosen in a way that all trajectory segments continue seamlessly.

The positions are calculated respectively in the same time intervals as in Equation (126):

$$p(t) = \begin{cases} p_F(t) = \widetilde{p_F}(t) + C_{p,F}, & 0 \le t \le t_{FT} \\ p_T(t) = \widetilde{p_T}(t) + C_{p,T}, & t_{FT} < t < t_{stop} \end{cases} \quad (126)$$

where the constants of integration must be chosen in a way that all trajectory segments fit together seamlessly, as noted in Equations (127) and (128):

$$C_{p,F} = p_0 - \widetilde{p_F}(0) \quad (127)$$

$$C_{p,T} = p_T(t_{FT}) - \widetilde{p_R}(t_{FT}) \quad (128)$$

See Figure 25b for a set of different Type H Trajectories. The model parameters and inputs are equal in all examples of Type H, except for the Braking Factor b, which is chosen to be in an admissible range to result in Type H Trajectories.

Trajectory Type I: The state changes for Type I Trajectories are defined by the simple sequence $t_{0,T} \rightarrow t_{stop,R}$ in Figure 14.

Figure 27 shows the yaw rate of a Type I Trajectory. The effective yaw rate is marked by a thick line to underline the simplicity of Type I trajectories.

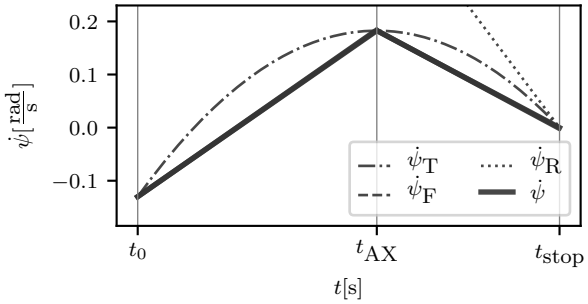

Figure 27. The yaw rates of a Type I trajectory. The effective yaw rate is marked by a thick line style.

The yaw angle function for all Type I trajectories is defined as Equation (129):

$$\psi(t) = \overline{\psi_T}(t) = \widetilde{\overline{\psi_T}}(t) + C_{\psi,T}, \quad t_0 \le t < t_{stop} \quad (129)$$

where the constant of integration must be chosen specific to this trajectory type as shown in Equation (130):

$$C_{\psi,T} = \psi_0 - \widetilde{\psi_T}(t_0) \quad (130)$$

The constant for $\Psi(t)$ is chosen in a way that the trajectory starts correctly with ψ_0.

The positions are calculated respectively in the same time intervals as in Equation (131):

$$p(t) = p_T(t) = \widetilde{p_T}(t) + C_{p,T}, \quad t_0 \le t < t_{stop} \quad (131)$$

where the constant of integration must be chosen in a way that the trajectory starts correctly at p_0, as noted in Equation (132):

$$C_{p,T} = p_0 - \widetilde{p_T}(t_0) \quad (132)$$

See Figure 28 for a set of different Type I Trajectories. The model parameters and inputs are equal in all examples of Type I, except for the Braking Factor b, which is chosen to be in an admissible range to result in Type I Trajectories. It can be seen that all trajectories are on top of each other, which makes sense, because the braking factor only has influence on the actual direction when the Friction Circle is involved in the calculation. In Type I trajectories this is not the case.

V. Conclusion

In this paper, we present two models for hard braking and collision avoiding vehicle trajectories. In the Basic Model, we take into account the maximally applicable acceleration/deceleration between tires and road surface, the minimal turning radius, the vehicle velocity, as well as starting position and heading. We explain our approach in detail and compare our model equations with an iterative CTRA-Model

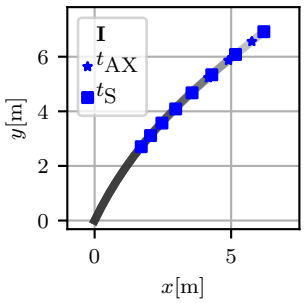

Figure 28. Eight trajectories of Type I. Note that since the Friction Circle has no influence in these trajectories, they are all located along the same path.

simulation, which finds very similar solutions. However, in tests we could show that our Basic Model computes stopping positions and trajectories up to 20 times faster than CTRA. The Extended Model furthermore take into account the initial yaw rate of a vehicle, as well as its ability to change the steering angle. In order to translate the steering angle into a yaw rate, we introduce the length of a vehicle and its turning direction. The increased complexity leads to 9 different trajectory types, which we explore in depth. By solving the compound differential equations of both models for position in x, y-plane, we describe the complete vehicle motion till full stop, while also turning and still respecting the Friction Circle. With the derived equations, we can directly compute possible positions that a vehicle will reach in a braking and collision avoiding scenario. This might be used to generate braking and collision avoiding trajectories, by sampling feasible motion primitives, which can be computed in very short time.

We contribute a Basic Model, which can aid in solving reachability problems for hard braking vehicles in an accurate and yet overapproximative way. Furthermore we contribute a second, Extended Model, which takes into account initial vehicle dynamics and respects further physical constraints. The second model is therefore much better suited for calculating motion primitives of actual emergency trajectories.

As next steps, the proposed models for vehicle motion can be compared to the trajectories of real vehicles under the same assumptions given. Another next step might be the usage of our model for fast generation of braking trajectories by sampling motion primitives and a comparison to other state of the art methods. We suggest to search a tree structure of connected motion primitives sampled from the Extended Model for feasible and yet complex evasive trajectories. As we can directly compute motion primitives for the highly non linear motions in braking and collision avoidance, the proposed model can significantly reduce valuable calculation time. Another application is the application of both models in a formal reachability analysis for risk assessment in hard braking traffic scenarios and compare the solution to other contributions in the field of reachability analysis.

References

[1] F. Terhar and C. Icking, "A New Model for Hard Braking Vehicles and Collision Avoiding Trajectories," in *Proceedings of the 8th International Conference on Advances in Vehicular Systems, Technologies and Applications*, June 2019, pp. 28–33.

[2] M. Werling, J. Ziegler, S. Kammel, and S. Thrun, "Optimal trajectory generation for dynamic street scenarios in a frenet frame," in *Proceedings - IEEE International Conference on Robotics and Automation*, 06 2010, pp. 987 – 993.

[3] J. Ziegler, M. Werling, and J. Schröder, "Navigating car-like robots in unstructured environments using an obstacle sensitive cost function," in *IEEE Intelligent Vehicles Symposium, Proceedings*, 07 2008, pp. 787 – 791.

[4] C. Pek and M. Althoff, "Computationally efficient fail-safe trajectory planning for self-driving vehicles using convex optimization," in *Proceedings of the IEEE International Conference on Intelligent Transportation Systems*, 2018, pp. 1447–1454.

[5] S. Magdici and M. Althoff, "Fail-safe motion planning of autonomous vehicles," in *2016 IEEE 19th International Conference on Intelligent Transportation Systems (ITSC)*, Nov 2016, pp. 452–458.

[6] C. Pek, M. Koschi, and M. Althoff, "An online verification framework for motion planning of self-driving vehicles with safety guarantees," in *AAET - Automatisiertes und vernetztes Fahren*, 01 2019, pp. 260–274.

[7] S. Heinrich, "Planning Universal On-Road Driving Strategies for Automated Vehicles." "Springer Fachmedien Wiesbaden", 2018, ch. 4, pp. 33–47.

[8] I. M. Mitchell, "Comparing forward and backward reachability as tools for safety analysis," in *Hybrid Systems: Computation and Control*, A. Bemporad, A. Bicchi, and G. Buttazzo, Eds., 2007, pp. 428–443.

[9] E. Asarin, T. Dang, and A. Girard, "Reachability analysis of nonlinear systems using conservative approximation," in *Hybrid Systems: Computation and Control*, O. Maler and A. Pnueli, Eds., 2003, pp. 20–35.

[10] A. Girard, "Reachability of uncertain linear systems using zonotopes," in *Hybrid Systems: Computation and Control*, M. Morari and L. Thiele, Eds., 2005, pp. 291–305.

[11] M. Koschi and M. Althoff, "SPOT: A tool for set-based prediction of traffic participants," in *2017 IEEE Intelligent Vehicles Symposium (IV)*, June 2017, pp. 1686–1693.

[12] M. Althoff, "Reachability analysis and its application to the safety assessment of autonomous cars," Dissertation, Technische Universität München, München, 2010.

[13] B. Kim *et al.*, "Probabilistic vehicle trajectory prediction over occupancy grid map via recurrent neural network," *CoRR*, vol. abs/1704.07049, 2017.

[14] F. Giovannini, G. Savino, and M. Pierini, "Influence of the minimum swerving distance on the development of powered two wheeler active braking," in *22nd ESV Conference*, June 2011, paper 11-0258.

[15] C. Ackermann, J. Bechtloff, and R. Isermann, "Collision avoidance with combined braking and steering," in *6th International Munich Chassis Symposium 2015*, P. Pfeffer, Ed., 2015, pp. 199–213.

[16] C. Choi and Y. Kang, "Simultaneous braking and steering control method based on nonlinear model predictive control for emergency driving support," *International Journal of Control, Automation and Systems*, vol. 15, no. 1, pp. 345–353, Feb 2017.

[17] J. Stewart, "Calculus: Early transcendentals," L. Covello, Ed. Thomson Brooks/Cole, 2010, ch. 5.

[18] H. B. Pacejka, "Chapter 1 - Tire characteristics and vehicle handling and stability," in *Tire and Vehicle Dynamics (Third edition)*, H. B. Pacejka, Ed., 2012.

[19] R. Schubert, E. Richter, and G. Wanielik, "Comparison and evaluation of advanced motion models for vehicle tracking," in *11th International Conference on Information Fusion*, June 2008, pp. 1–6.

[20] S. Söntges and M. Althoff, "Computing the drivable area of autonomous road vehicles in dynamic road scenes," *IEEE Transactions on Intelligent Transportation Systems*, vol. 19, no. 6, pp. 1855–1866, June 2018.

[21] "*NIST Digital Library of Mathematical Functions*," http://dlmf.nist.gov/, Release 1.0.25 of 2019-12-15, f. W. J. Olver, A. B. Olde Daalhuis, D. W. Lozier, B. I. Schneider, R. F. Boisvert, C. W. Clark, B. R. Miller, B. V. Saunders, H. S. Cohl, and M. A. McClain, eds.

[22] I. Stewart, "Taming the Infinite: The Story of Mathematics from the First Numbers to Chaos Theory." Quercus, 2008, ch. 4.